MMS Observations of a Compressed Current Sheet: Importance of the Ambipolar Electric Field

Ami M. DuBois, Chris Crabtree, Gurudas Ganguli, David M. Malaspina, and William E. Amatucci

Phys. Rev. Lett. **129**, 105101 — Published 2 September 2022

DOI: 10.1103/PhysRevLett.129.105101

MMS Observations of a Compressed Current Sheet: Importance of the Ambipolar Electric Field

Ami M. DuBois[1], Chris Crabtree[1], Gurudas Ganguli[1], David M. Malaspina[2,3], William E. Amatucci[1]
[1]*U.S. Naval Research Laboratory, Plasma Physics Division, Washington, D.C. 20375-5346, USA*
[2]*Astrophysical and Planetary Sciences Department, University of Colorado, Boulder, CO 80303-7814, USA*
[3]*Laboratory for Atmospheric and Space Physics, University of Colorado, Boulder, CO, 80303-7814, USA*

(Received; accepted; published)

Spacecraft data reveals a non-uniform ambipolar electric field transverse to the magnetic field in a thin current sheet in the Earth's magnetotail that leads to intense **E**×**B** velocity shear and non-gyrotropic particle distributions. The **E**×**B** drift far exceeds the diamagnetic drift so that the sheared drift drives lower hybrid waves localized to the magnetic field reversal region, which is ideally suited for the anomalous dissipation necessary for reconnection. It also reveals substructures embedded in the current density, indicating a compressed current sheet.

DOI:

Current sheets are important to space and laboratory plasmas [1–6], and particularly to the Earth's magnetotail. A consequential but overlooked feature of thin current sheets is a transverse ambipolar electric field which is self-consistently generated as the magnetotail is compressed by the solar wind. [7] This interaction of large and small-scale physics may consist of turbulent processes forming plasmoids and flux ropes, etc. [8,9] with kinetic-scale current sheets between them that can reorganize the macroscopic magnetic topology through reconnection and affect the magnetospheric plasma environment, also known as "space weather". *In situ* measurements have shown compression of the magnetotail creates thin current sheets of widths comparable to the ion gyro-radius (ρ_i), occasionally with single [10–12] or double peaked [13–17] substructures embedded in the current density. These thin structured current sheets cannot be explained by the standard Harris equilibrium [18], which is commonly used as an ideal current sheet representation [6]. Intense lower hybrid (LH) wave activity and subsequent magnetic reconnection with large scale topological changes is also observed, which may result in a plasma dipolarization front accelerating towards Earth, injecting energetic particles into the radiation belts [19–24], followed by a redistribution of mass, energy, and momentum throughout the magnetosphere [6,7,16,25–28] which impacts Earth orbiting satellites. It is therefore critical to understand the physics of thin structured current sheets, especially the kinetic structures within, and the associated dynamics. The formation of the ambipolar electric field in thin current sheets at the smallest scale can affect particle orbits and provides a new mechanism to generate intense electrostatic turbulence near the magnetic field reversal, resulting in anomalous dissipation processes that can initiate magnetic reconnection.

Theoretical [7,29,30] and laboratory [31–33] studies have shown that velocity-shear can intensify due to the ambipolar electric field generated by plasma compression, driving broadband turbulence peaking at the LH frequency. Shear-driven LH waves dominate over the LH drift (LHD) instability at the center of the current sheet where the density is nearly flat [34] and the shear frequency, defined as the spatial derivative of the $\vec{E} \times \vec{B}$ flow, exceeds the diamagnetic drift frequency. [7,35,36] Identification of shear-driven LH waves in *in situ* data is not only evidence of a thin structured current sheet, but also emphasizes the importance of the ambipolar electric field [7], the scope of which has not been explored in previous magnetotail investigations [37–42]. As the scale size of the current sheet becomes comparable to ρ_i, the electric field intensifies making the velocity-shear strong, which can explain many observed features and their causality, such as non-gyrotropic distributions [7,16,28,43,44], plasma heating and cooling [7,27,41], vortex structures [7,20,35,45,46], and the wide bandwidth of spectral signatures [7,32]. The ability of the ambipolar electric field to break gyrotropy is an indicator of its major role in reconnection [47–49]. This letter presents the first evidence of shear-driven LH waves resulting from global compression that demonstrates the significance of transverse ambipolar electric fields in thin current sheets that can occur prior to reconnection.

The four Magnetospheric Multi-Scale (MMS) spacecraft [50] traversed a current sheet (an approximate 1D plasma structure near a magnetic reversal) in the Earth's magnetotail on July 3, 2017 and crossed the null point at approximately 5:27:07.02 UTC. Rotating the vector data into a frame normal to the current sheet (LMN

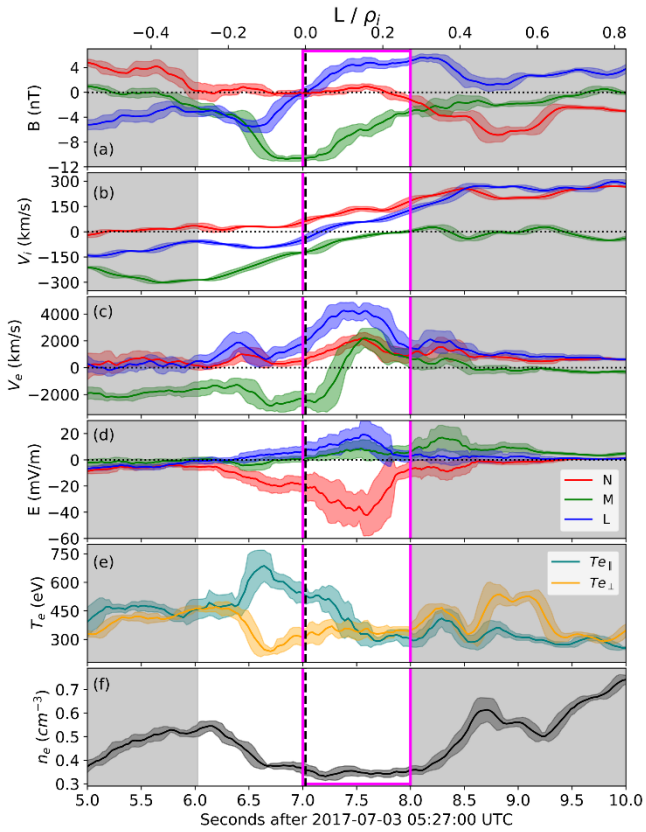

FIG. 1. Boxcar averaged MMS1 plasma parameters as a function of time (bottom axis) and distance normalized to ρ_i = 841 km (top axis). (a) Magnetic field burst data (128 S/s) measured by the fluxgate magnetometer [51], (b) ion velocity, (c) electron velocity, and (d) electric field burst data (8192 S/s) measured by FIELDS [52] rotated into LMN coordinates (blue=$\hat{L}$, green=$\hat{M}$, red=$\hat{N}$), (e) parallel (teal) and perpendicular (orange) electron temperature, and (f) electron density. Velocities, densities, and temperatures are obtained from the fast plasma investigation (FPI) [53] burst measurements (ions = 6 S/s, electrons = 33 S/s). The unshaded region highlights ±1 second around the B_L reversal (vertical dashed line), around which the electron diffusion region is typically located. The magenta box indicates the region during which electrostatic LH fluctuations are present.

coordinates) allows for the analysis below, which suggests that an ambipolar electric field forms due to compression of the current sheet, with an $\vec{E} \times \vec{B}$ shear flow associated with LH fluctuations. The density gradient is small in this region, suggesting that the shear flow provides the energy for the fluctuations.

During this event, the MMS spacecraft are in the night-side of Earth's plasma sheet on the dusk side of midnight far from the magnetopause. Using the magnetic field measurements between 6 and 8 seconds, minimum variance analysis (MVA) [54,55] is used to calculate the eigenvector corresponding to a direction normal ($\hat{N}$) to the current sheet. The angular difference between the averaged eigenvector and the eigenvectors calculated individually from each spacecraft ($\cos^{-1}(\hat{n}_{avg} \cdot \hat{n}_i)$) is small (<4°), which is a good indicator that the magnetic field gradient is much stronger in $\hat{N}$ compared to other directions. Additionally, a guide for judging the quality of the MVA is a large ratio of the eigenvalues corresponding to the $\hat{M}$ and $\hat{N}$ directions, (λ_M/λ_N=12) indicating a well-defined $\hat{N}$ direction [52]. The resulting transformation matrix from GSE coordinates is [L,M,N] = [[-0.67,-0.68,-0.30], [-0.70,0.71,-0.04], [-0.24,-0.18,0.95]]. The vector data presented henceforth are rotated into LMN coordinates using the transformation matrix in order to better infer measurements with respect to the orientation of the current sheet such that $\hat{N}$ is normal to the current sheet, $\hat{L}$ is in the direction whose magnetic component reverses sign, and $\hat{M}$ is the direction of the guide magnetic field.

A summary of the MMS1 data for a 5 s time span during the current sheet crossing is shown in Fig. 1. Data from each spacecraft are comparable with similar features, so only MMS1 data are shown. A boxcar averaging low pass filter routine is applied to the time series measurements to improve the signal to noise ratio and smooth the data to infer quasi-static profiles. The top axis displays time converted to distance and normalized to a representative ρ_i (calculated from the average of the total magnetic field and ion temperature between 7 and 8 s) to show how features compare to ion-scale sizes. To convert time to distance, we use the fact that the current sheet is sweeping by in $\hat{N}$ much faster than the spacecraft are moving (V_{MMS} = 1.47 km/s). The magnetic field data from each spacecraft are shifted in time to align the B_L reversals. With the timing information and the spacecraft locations relative to each other, the current sheet velocity can be estimated as V_{cs} = 223.1 ± 57.5 km/s $\hat{N}$. The time (x-axis) is then multiplied by V_{cs} to convert to distance, and then normalized to ρ_i.

The magnetic field LMN components in Fig. 1(a) show that by rotating the data into a frame normal to the current sheet, B_N is near-zero with a B_L reversal at 7.02 s (dashed, vertical line), which indicates the current sheet crossing. The measured quantities are not symmetric about the B_L reversal. There is a guide field (B_M) of approximately 10 nT at the time of B_L reversal. Using the average total magnetic field between 7 and 8 s (magenta box), ρ_i = 841 km and ρ_e = 6.9 km (electron gyro-radius). The ion velocity [Fig. 1(b)] is significantly smaller than the electron velocity [Fig. 1(c)], indicating that the ions experience negligible electric field due to gyro averaging as the electric field scale size is less than ρ_i [7]. The total electron flow velocity, V_{eL}, has a scale size less than ρ_i. The electric field components are shown in Fig. 1(d), where E_L and E_M are both small compared to E_N (ambipolar electric field normal to the current sheet), which has a scale size less than ρ_i and peaks at -45 mV/m. The electron temperatures (T_e) and density (n_e) are shown in Figs. 1(e) and (f). In the region of peak E_N, n_e is nearly constant but exhibits a gradient at approximately 6.5 and 8.5 s.

Electrostatic fluctuation spectra are calculated by taking a spectrogram [55] of the E_N burst measurement data prior to boxcar averaging. All panels in Fig. 2 show electrostatic

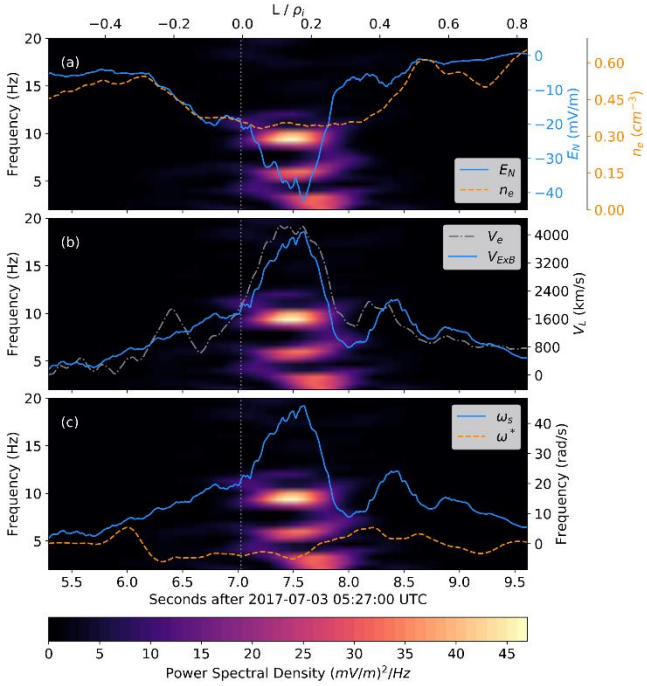

FIG. 2. Spectrogram showing power spectral density of electrostatic LH fluctuations as a function of time with (a) E_N (solid, blue) and n_e (dashed, orange) (b) total electron (gray, dot-dashed) and $\vec{E}\times\vec{B}$ shear (blue, solid) velocities in $\hat{L}$, (c) shear (blue, solid) and diamagnetic drift (dashed, orange) frequencies overlaid. The top axis shows distance normalized to ρ_i. The vertical dotted line indicates the B_L reversal time.

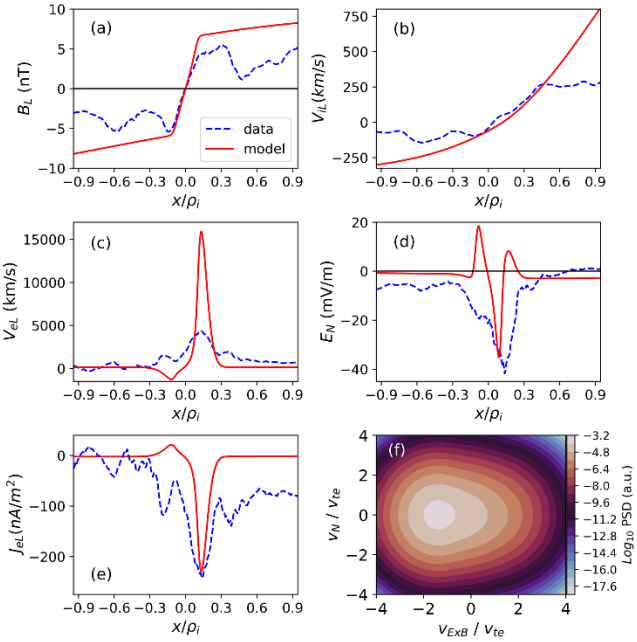

FIG. 3. Kinetic equilibrium model (solid, red) compared to MMS data (dashed, blue) as a function of distance normalized to ρ_i for (a) magnetic field in $\hat{L}$, (b) ion velocity in $\hat{L}$, (c) electron velocity in $\hat{L}$ (d) ambipolar electric field in $\hat{N}$, (e) electron current density in $\hat{L}$. (f) The modeled non-gyrotropic electron distribution function that arises due to the ambipolar electric field, where the axes represent the electron flow in the direction of E_N (vertical) and parallel to $V_{E\times B}\hat{L}$ (horizontal) normalized to the thermal velocity. The color bar represents the log of the phase space density in arbitrary units.

fluctuations from 2 to 20 Hz, where color specifies the power spectral density such that black indicates instrument noise level and yellow indicates large amplitude fluctuations. The LH frequency ($f_{LH} = \frac{1}{2\pi}\sqrt{\omega_{ci}\omega_{ce}}$) at the B_L reversal is 7 Hz. The peak fluctuations occur at 7.5 s with a frequency of approximately 10 Hz, indicating these are LH waves. The boxcar averaged E_N (solid, blue) and n_e (dashed, orange) are overlaid on the fluctuation spectra [Fig. 2(a)] showing that E_N peaks during the largest amplitude fluctuations. The n_e is nearly constant during the time of fluctuations, and when there is a gradient, no LH fluctuations are observed. There is a large $\vec{E}\times\vec{B}$ velocity shear in $\hat{L}$ direction [Fig. 2(b), solid blue], where the wave activity peaks. The total electron flow in $\hat{L}$, V_{eL} [Fig. 2(b), gray dot-dashed], is in the same direction as $V_{E\times B}$, indicating that the electrons are $\vec{E}\times\vec{B}$ drifting. Additionally, because V_{eL} and $V_{E\times B}$ are close in magnitude, the diamagnetic drift velocity ($\vec{V}_{drift} = \nabla P_e \times \vec{B}/(n_e B^2)$) in the region of the wave localization is small compared to the $\vec{E}\times\vec{B}$ velocity. This indicates that the LH waves are driven by the sheared flow and not a density gradient.

The origin of the observed features can be gleaned from our kinetic model [7,56], which is extended to include a guide field [57]. Although the model includes magnetic field components in the y- and z-directions, it uses a WKB type ansatz, incorporating the strongest observed variation in the x-direction, perpendicular to the magnetic field. It constructs an exact solution to the Vlasov-Maxwell equations for species α by generalizing the Harris model to include an inhomogeneous guiding-center distribution,

$$f_{0\alpha} = \frac{N_{0\alpha}}{(\pi v_{t\alpha}^2)^{\frac{3}{2}}} Q_\alpha(\Upsilon_\alpha,\zeta_\alpha) e^{-\frac{E_\alpha - U_\alpha p_y - V_\alpha p_z + \frac{1}{2}m_\alpha U_\alpha^2 + \frac{1}{2}m_\alpha V_\alpha^2}{T_\alpha}} \quad (1)$$

where $Q_\alpha(\Upsilon_\alpha,\zeta_\alpha) = G(\Upsilon_\alpha) + H(\zeta_\alpha)$,

$$G(\Upsilon_\alpha) = \frac{1}{2}\left[R_{y\alpha} + S_{y\alpha} + (S_{y\alpha} - R_{y\alpha})Erf\left(\frac{\Upsilon_\alpha - \Upsilon_0}{L_{y\alpha}}\right)\right],$$

$$H(\zeta_\alpha) = R_{z\alpha} + (S_{z\alpha} - R_{z\alpha})Exp\left(-\frac{(\zeta_\alpha - \zeta_0)^2}{L_{z\alpha}^2}\right),$$

$\Upsilon_\alpha = [A_y(x)/B_0 + v_y/\Omega_\alpha]$ and $\zeta_\alpha = [A_z(x)/B_0 - B_v x + v_z/\Omega_\alpha]$ are the canonical momenta, $N_{o\alpha}S_\alpha$ and $N_{o\alpha}R_\alpha$ are asymptotic densities on the high/low sides of the guiding center distributions, G and H, and B_v is the vacuum component (due to external currents) of the guide field. The quasi-neutrality condition gives the electrostatic potential and Ampere's law gives the vector potential. This allows inhomogeneous structures in the moments (e.g. density, current, temperature, flows) to self-consistently develop in response to compression, which is represented by the scale sizes $L_{y\alpha}$ and $L_{z\alpha}$ of G and H, similar to the case with no guide field described in [7]. The current sheet

evolves on slow fluid time scales under compression, but the instability (Fig. 4) time scale is much faster. Hence, a stationary Vlasov solution is a reasonable assumption for understanding the wave effects. However, a simulation initialized by Eq. (1) can provide a more accurate picture of the dynamics. Using the parameters provided in the supplemental material [55], Fig. 3 compares MMS1 data (dashed, blue) to the model (solid, red) for (a) B_L, (b) V_{iL}, (c) V_{eL}, (d) E_N, and (e) electron current density in $\hat{L}$. It shows that as a broad Harris-type current sheet undergoes global compression, an ambipolar electric field (E_N) self-consistently develops. This produces a sheared $\vec{E} \times \vec{B}$ velocity, enabling shear-driven waves to arise in thin current sheets. The presence of a guide magnetic field introduces sheared parallel flows, $V_{||} = (\vec{E} \times \vec{B})/B^2 \cdot \hat{b}_{L,M}$, which can also drive waves [7]. Additionally, the bidirectional V_{iL} flow profile is found to be a stationary Vlasov solution and therefore may not imply occurrence of magnetic reconnection, as claimed [20]. Given the boundary conditions from the *in situ* measurements, the equilibrium model agrees with the general trends of the measurements. The observed profiles are relaxed because of the instability.

Our model also shows that as current sheets are compressed to scales less than ρ_i, substructures embedded in the current density can form, which cannot be explained by the standard Harris equilibrium. The current density (J) is calculated from MMS FPI data ($\vec{J} = en_i\vec{V}_i - en_e\vec{V}_e$), where the electron term dominates ($V_i << V_e$). Since $B_M > B_L$, the electron current density in $\hat{L}$, J_{eL}, is dominant and is comparable to the cross-field Hall current, $J \approx en(E_N \times B_M)$. Fig. 3(e) shows the J_{eL} data (dashed, blue) and model (solid, red). The large peak in J_{eL} is localized to the region of E_N and the waves. Both the data and model suggest the formation of a thin current sheet that has substructures contained within.

A distinguishing property of our equilibrium model is the formation of agyrotropy in distribution functions [7], which has been seen in this event but was thought to be a wave heating effect [20]. Fig. 3(f) shows the electron distribution function from the model, where the vertical axis is the electron flow in the direction along E_N and the horizontal axis is the direction of $V_{E\times B}\hat{L}$, both normalized to the thermal velocity. The agyrotropy arises in the equilibrium distribution function due to the ambipolar electric field.

Velocity shear can drive LH waves even in the presence of a pressure gradient as long as the shear frequency ($\omega_s \sim |\vec{V}_{E\times B}|/L_E$) is greater than the diamagnetic drift frequency ($\omega^* = -k_\perp \vec{V}_{drift}$) [7,29,35,36,56]. The shear scale length (L_E) can be estimated by taking the half-width at half-max of the boxcar averaged E_N. The average L_E is estimated to be 89 ± 23 km such that $\rho_e < L_E < \rho_i$. Following Norgren et al. [46], $k_\perp$ is calculated by first finding the time shift

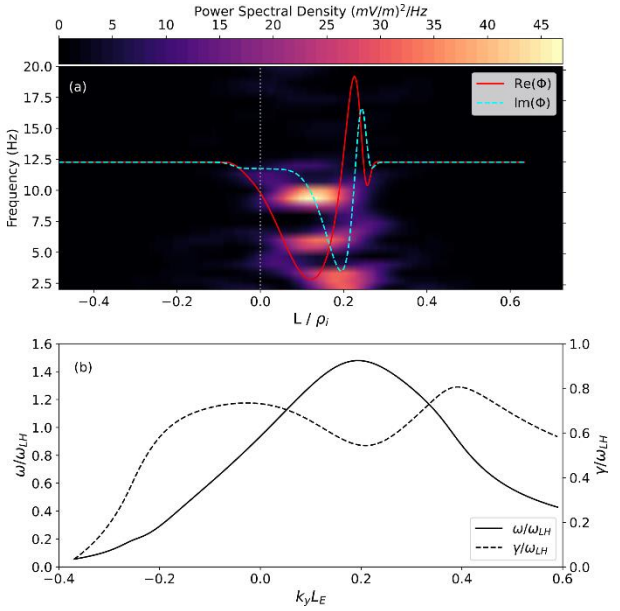

FIG. 4. (a) Spectrogram showing power spectral density of electrostatic LH fluctuations as a function of distance normalized to ρ_i with the real (solid, red) and imaginary (dashed, blue) eigenmodes, ϕ, overlaid. The vertical dotted line indicates the B_L reversal. (b) The frequency (solid) and growth rate (dashed) normalized to ω_{LH} plotted as a function of k_yL_E.

between E_L measured from MMS1 and MMS2 (largest separation in $\hat{L}$). The wave phase speed is calculated using the distance in $\hat{L}$ between MMS1 and MMS2 and the time shift between the signals. The phase speed is then used to calculate the fluctuation wavelength, $k_\perp = \frac{2\pi}{\lambda} = 0.027 \pm 0.01\ km^{-1}$. Fig. 2(c) shows that ω_s (blue, solid) is an order of magnitude larger than ω^* (orange, dashed), indicating that the velocity shear is the dominating energy source for the waves. The Electron-Ion Hybrid (EIH) instability is driven by the free energy provided by sheared flows [7,33,36,58] and characterized by $k_\perp\rho_e \ll 1$ and $k_\perp L_E \sim 1$. Observations from this event give $k_\perp\rho_e = 0.18 \pm 0.07$ and $k_\perp L_E = 2.4 \pm 1.2$ reinforcing that the character of the LH fluctuations are consistent with EIH instability and not the LHD instability. Vortices, reported earlier for this event [20], are also a natural consequence of the velocity shear that drives the EIH waves [35].

In order to compare this dataset with theory, we generalized the nonlocal theory of the EIH instability [59] to include a guide field and magnetic field reversal. A model equilibrium electric field, consistent with the observed E_N, is used to drive sheared flows in V_L and V_M. The parameters [55] used to solve the eigenvalue problem are consistent with observations. The eigenfunction corresponding to the EIH mode with the maximum growth rate is localized around the strong V_L flow near the center of the current sheet [Fig. 4(a)], also consistent with observations. Solution of the eigenmode condition as a function of k_L normalized by L_E provides the growth rate and frequency [Fig. 4(b)] normalized to ω_{LH}, indicating a

large domain of the shear driven instability ideally located in the center of the current sheet for anomalous dissipation [35,60,61] to trigger reconnection.

In summary, *in situ* measurements show a localized ambipolar electric field develops in a thin current sheet and results in a strong sheared $\vec{E} \times \vec{B}$ velocity, which drives LH fluctuations, with a negligible density gradient. The ambipolar electric field breaks gyrotropy in the distribution function and drives waves capable of producing anomalous resistivity that can determine the reconnection rate. This implies a seamless connection of the local reconnection rate with the global compression. With further research, it will be possible to develop a parameterization of the anomalous resistivity suitable for fluid models to trigger reconnection for realistic parameters consistent with global forcing. Since 3D PIC simulations with large scales and mass ratios needed to capture the essential physics are expensive, fluid models with a parameterization of the kinetic effects is an optimal way to explore the larger-scale physics with local kinetic feedback.

The frozen-in condition may be broken by anomalous resistivity. However, the off-diagonal terms in the pressure tensor can also play a role [40,59,60]. Interestingly, off-diagonal terms may also be generated by compression, as was argued for dipolarization fronts [64]. Using our kinetic equilibrium as the initial condition in PIC simulations could help reveal the impact of thin structured current sheets and the associated dynamics on reconnection, and the relative roles of anomalous resistivity and off-diagonal components of the pressure tensor. These are interesting topics for further research.

This work was supported by the Naval Research Laboratory Base Program. All MMS data used in this work are publically available and can be found online (https://lasp.colorado.edu/mms/sdc/public).

---

[1] M. Yamada, R. Kulsrud, and H. Ji, *Magnetic Reconnection*, Rev. Mod. Phys. **82**, 603 (2010).

[2] J. Chen, *Physics of the Magnetotail Current Sheet*, Physics of Fluids B **5**, 2663 (1993).

[3] C. Chen, Y. D. Liu, and H. Hu, *Macro Magnetic Holes Caused by Ripples in Heliospheric Current Sheet from Coordinated Imaging and Parker Solar Probe Observations*, The Astrophysical Journal **921**, 1 (2021).

[4] L. P. Chitta, E. R. Priest, and X. Cheng, *From Formation to Disruption: Observing the Multiphase Evolution of a Solar Flare Current Sheet*, The Astrophysical Journal **911**, 133 (2021).

[5] L. B. Wilson, A. L. Brosius, N. Gopalswamy, T. Nieves-Chinchilla, A. Szabo, K. Hurley, T. Phan, J. C. Kasper, N. Lugaz, I. G. Richardson, C. H. K. Chen, D. Verscharen, R. T. Wicks, and J. M. TenBarge, *A Quarter Century of Wind Spacecraft Discoveries*, Reviews of Geophysics **59**, 1 (2021).

[6] A. Petrukovich, A. Artemyev, I. Vasko, R. Nakamura, and L. Zelenyi, *Current Sheets in the Earth Magnetotail: Plasma and Magnetic Field Structure with Cluster Project Observations*, Space Science Reviews **188**, 311 (2015).

[7] G. Ganguli, C. Crabtree, A. Fletcher, and B. Amatucci, *Behavior of Compressed Plasmas in Magnetic Fields*, Reviews of Modern Plasma Physics **4**, 1 (2020).

[8] D. A. Uzdensky, N. F. Loureiro, and A. A. Schekochihin, *Fast Magnetic Reconnection in the Plasmoid-Dominated Regime*, Phys. Rev. Lett. **105**, 235002 (2010).

[9] W. Daughton, V. Roytershteyn, H. Karimabadi, L. Yin, B. J. Albright, B. Bergen, and K. J. Bowers, *Role of Electron Physics in the Development of Turbulent Magnetic Reconnection in Collisionless Plasmas*, Nature Physics **7**, 539 (2011).

[10] D. J. McComas, C. T. Russell, R. C. Elphic, and S. J. Bame, *The Near-Earth Cross-Tail Current Sheet: Detailed ISEE 1 and 2 Case Studies*, Journal of Geophysical Research **91**, 4287 (1986).

[11] A. A. Petrukovich, A. V. Artemyev, H. V. Malova, V. Y. Popov, R. Nakamura, and L. M. Zelenyi, *Embedded Current Sheets in the Earth's Magnetotail*, Journal of Geophysical Research **116**, A00I25 (2011).

[12] V. I. Domrin, H. V. Malova, A. V. Artemyev, and A. P. Kropotkin, *Peculiarities of the Formation of a Thin Current Sheet in the Earth's Magnetosphere*, Cosmic Research **54**, 423 (2016).

[13] K. Schindler and M. Hesse, *Formation of Thin Bifurcated Current Sheets by Quasisteady Compression*, Physics of Plasmas **15**, 042902 (2008).

[14] M. Hoshino, A. Nishida, T. Mukai, Y. Saito, T. Yamamoto, and S. Kokubun, *Structure of Plasma Sheet in Magnetotail: Double-Peaked Electric Current Sheet*, Journal of Geophysical Research **101**, 24775 (1996).

[15] Y. Asano, T. Mukai, M. Hoshino, Y. Saito, H. Hayakawa, and T. Nagai, *Current Sheet Structure around the Near-Earth Neutral Line Observed by Geotail*, Journal of Geophysical Research: Space Physics **109**, 1 (2004).

[16] C. Norgren, D. B. Graham, Y. V. Khotyaintsev, M. André, A. Vaivads, M. Hesse, E. Eriksson, P. A. Lindqvist, B. Lavraud, J. Burch, S. Fuselier, W. Magnes, D. J. Gershman, and C. T. Russell, *Electron Reconnection in the Magnetopause Current Layer*, Journal of Geophysical Research: Space Physics **123**, 9222 (2018).

[17] A. Runov, R. Nakamura, W. Baumjohann, T. L. Zhang, M. Volwerk, H. U. Eichelberger, and A. Balogh, *Cluster Observation of a Bifurcated Current Sheet*, Geophysical Research Letters **30**, 1036 (2003).

[18] E. G. Harris, *On a Plasma Sheath Separating Regions of Oppositely Directed Magnetic Field*, Il Nuovo Cimento **23**, 115 (1962).

[19] D. A. Gurnett, L. A. Frank, and R. P. Lepping, *Plasma Waves in the Distant Magnetotail*, Journal of Geophysical Research **81**, 6059 (1976).

[20] L. J. Chen, S. Wang, O. Le Contel, A. Rager, M. Hesse, J. Drake, J. Dorelli, J. Ng, N. Bessho, D. Graham, L. B. Wilson, T. Moore, B. Giles, W. Paterson, B. Lavraud, K. Genestreti, R. Nakamura, Y. V. Khotyaintsev, R. E. Ergun, R. B. Torbert, J. Burch, C. Pollock, C. T. Russell, P. A. Lindqvist, and L. Avanov, *Lower-Hybrid Drift Waves Driving Electron Nongyrotropic Heating and Vortical Flows in a Magnetic Reconnection Layer*, Physical Review Letters **125**, 025103 (2020).

[21] S. Ohtani, H. Korth, P. C. Brandt, L. G. Blomberg, H. J. Singer, M. G. Henderson, E. A. Lucek, H. U. Frey, Q. Zong, J. M. Weygand, Y. Zheng, and A. T. Y. Lui, *Cluster Observations in the Inner Magnetosphere during the 18 April 2002 Sawtooth Event: Dipolarization and Injection at r = 4.6 RE*, Journal of Geophysical Research **112**, A08213 (2007).

[22] R. Nakamura, W. Baumjohann, Y. Asano, A. Runov, A. Balogh, C. J. Owen, A. N. Fazakerley, M. Fujimoto, B. Klecker, and H. Rème, *Dynamics of Thin Current Sheets Associated with Magnetotail Reconnection*, Journal of Geophysical Research: Space Physics **111**, A11206 (2006).

[23] M. Nosé, H. Koshiishi, H. Matsumoto, P. Cson Brandt, K. Keika, K. Koga, T. Goka, and T. Obara, *Magnetic Field Dipolarization in the Deep Inner Magnetosphere and Its Role in Development of O+-Rich Ring Current*, Journal of Geophysical Research: Space Physics **115**, A00J03 (2010).

[24] Y. Xu, H. S. Fu, C. Norgren, K. J. Hwang, and C. M. Liu,

Formation of Dipolarization Fronts after Current Sheet Thinning, Physics of Plasmas **25**, 072123 (2018).

[25] R. Nakamura, W. Baumjohann, A. Runov, M. Volwerk, T. L. Zhang, B. Klecker, Y. Bogdanova, A. Roux, A. Balogh, H. Rème, J. A. Sauvaud, and H. U. Frey, *Fast Flow during Current Sheet Thinning*, Geophysical Research Letters **29**, 2140 (2002).

[26] Y. Asano, T. Mukai, M. Hoshino, Y. Saito, H. Hayakawa, and T. Nagai, *Statistical Study of Thin Current Sheet Evolution around Substorm Onset*, Journal of Geophysical Research: Space Physics **109**, 1 (2004).

[27] J. Liang, W. W. Liu, and E. F. Donovan, *Ion Temperature Drop and Quasi-Electrostatic Electric Field at the Current Sheet Boundary Minutes Prior to the Local Current Disruption*, Journal of Geophysical Research: Space Physics **114**, A10215 (2009).

[28] S. Lu, R. Wang, Q. Lu, V. Angelopoulos, R. Nakamura, A. V. Artemyev, P. L. Pritchett, T. Z. Liu, X. J. Zhang, W. Baumjohann, W. Gonzalez, A. C. Rager, R. B. Torbert, B. L. Giles, D. J. Gershman, C. T. Russell, R. J. Strangeway, Y. Qi, R. E. Ergun, P. A. Lindqvist, J. L. Burch, and S. Wang, *Magnetotail Reconnection Onset Caused by Electron Kinetics with a Strong External Driver*, Nature Communications **11**, 5049 (2020).

[29] G. Ganguli, M. J. Keskinen, H. Romero, R. Heelis, T. Moore, and C. Pollock, *Coupling of Microprocesses and Macroprocesses Due to Velocity Shear: An Application to the Low-Altitude Ionosphere*, Journal of Geophysical Research **99**, 8873 (1994).

[30] H. Romero and G. Ganguli, *Relaxation of the Stressed Plasma Sheet Boundary Layer*, Geophysical Research Letters **21**, 645 (1994).

[31] A. M. DuBois, E. Thomas, Jr., W. E. Amatucci, and G. Ganguli, *Plasma Response to a Varying Degree of Stress*, Phys. Rev. Lett. **111**, 145002 (2013).

[32] A. M. DuBois, E. Thomas, W. E. Amatucci, and G. Ganguli, *Experimental Characterization of Broadband Electrostatic Noise Due to Plasma Compression*, J. Geophys. Res.: Space Phys. **119**, 5624 (2014).

[33] W. E. Amatucci, G. Ganguli, D. N. Walker, G. Gatling, M. Balkey, and T. McCulloch, *Laboratory Investigation of Boundary Layer Processes Due to Strong Spatial Inhomogeneity*, Physics of Plasmas **10**, 1963 (2003).

[34] A. Runov, V. A. Sergeev, R. Nakamura, W. Baumjohann, S. Apatenkov, Y. Asano, T. Takada, M. Volwerk, Z. Vörös, T. L. Zhang, J. A. Sauvaud, H. Rème, and A. Balogh, *Local Structure of the Magnetotail Current Sheet: 2001 Cluster Observations*, Annales Geophysicae **24**, 247 (2006).

[35] H. Romero and G. Ganguli, *Nonlinear Evolution of a Strongly Sheared Cross-Field Plasma Flow*, Physics of Fluids B **5**, 3163 (1993).

[36] A. M. DuBois, E. Thomas, W. E. Amatucci, and G. Ganguli, *Density Gradient Effects on Transverse Shear Driven Lower Hybrid Waves*, Physics of Plasmas **21**, 062117 (2014).

[37] M. I. Sitnov, P. N. Guzdar, and M. Swisdak, *A Model of the Bifurcated Current Sheet*, Geophysical Research Letters **30**, 1712 (2003).

[38] J. Birn, K. Schindler, and M. Hesse, *Thin Electron Current Sheets and Their Relation to Auroral Potentials*, Journal of Geophysical Research **109**, A02217 (2004).

[39] P. H. Yoon and A. T. Y. Lui, *Model of Ion- or Electron-Dominated Current Sheet*, Journal of Geophysical Research **109**, A11213 (2004).

[40] M. I. Sitnov, M. Swisdak, P. N. Guzdar, and A. Runov, *Structure and Dynamics of a New Class of Thin Current Sheets*, Journal of Geophysical Research **111**, A08204 (2006).

[41] W. W. Liu, J. Liang, and E. F. Donovan, *Electrostatic Field and Ion Temperature Drop in Thin Current Sheets: A Theory*, Journal of Geophysical Research **115**, A03211 (2010).

[42] J. Egedal, J. Ng, A. Le, W. Daughton, B. Wetherton, J. Dorelli, D. Gershman, and A. Rager, *Pressure Tensor Elements Breaking the Frozen-In Law during Reconnection in Earth's Magnetotail*, Physical Review Letters **123**, 225101 (2019).

[43] M. Zhou, X. H. Deng, Z. H. Zhong, Y. Pang, R. X. Tang, M. El-Alaoui, R. J. Walker, C. T. Russell, G. Lapenta, R. J. Strangeway, R. B. Torbert, J. L. Burch, W. R. Paterson, B. L. Giles, Y. V. Khotyaintsev, R. E. Ergun, and P.-A. Lindqvist, *Observations of an Electron Diffusion Region in Symmetric Reconnection with Weak Guide Field*, The Astrophysical Journal **870**, 34 (2019).

[44] R. Nakamura, K. J. Genestreti, T. Nakamura, W. Baumjohann, A. Varsani, T. Nagai, N. Bessho, J. L. Burch, R. E. Denton, J. P. Eastwood, R. E. Ergun, D. J. Gershman, B. L. Giles, H. Hasegawa, M. Hesse, P. A. Lindqvist, C. T. Russell, J. E. Stawarz, R. J. Strangeway, and R. B. Torbert, *Structure of the Current Sheet in the 11 July 2017 Electron Diffusion Region Event*, Journal of Geophysical Research: Space Physics **124**, 1173 (2019).

[45] S. Wang, L. J. Chen, J. Ng, N. Bessho, and M. Hesse, *Lower-Hybrid Drift Waves and Their Interaction with Plasmas in a 3D Symmetric Reconnection Simulation with Zero Guide Field*, Physics of Plasmas **28**, 072102 (2021).

[46] C. Norgren, A. Vaivads, Y. V. Khotyaintsev, and M. André, *Lower Hybrid Drift Waves: Space Observations*, Physical Review Letters **109**, 055001 (2012).

[47] S. M. Mahajan and R. D. Hazeltine, *Sheared-Flow Generalization of the Harris Sheet*, Physics of Plasmas **7**, 1287 (2000).

[48] J. D. Scudder and F. S. Mozer, *Electron Demagnetization and Collisionless Magnetic Reconnection in Be $\ll$1 Plasmas*, Physics of Plasmas **12**, 092903 (2005).

[49] J. Scudder and W. Daughton, *Illuminating Electron Diffusion Regions of Collisionless Magnetic Reconnection Using Electron Agyrotropy*, Journal of Geophysical Research **113**, A06222 (2008).

[50] J. L. Burch, T. E. Moore, R. B. Torbert, and B. L. Giles, *Magnetospheric Multiscale Overview and Science Objectives*, Space Science Reviews **199**, 5 (2016).

[51] C. T. Russell, B. J. Anderson, W. Baumjohann, K. R. Bromund, D. Dearborn, D. Fischer, G. Le, H. K. Leinweber, D. Leneman, W. Magnes, J. D. Means, M. B. Moldwin, R. Nakamura, D. Pierce, F. Plaschke, K. M. Rowe, J. A. Slavin, R. J. Strangeway, R. Torbert, C. Hagen, I. Jernej, A. Valavanoglou, and I. Richter, *The Magnetospheric Multiscale Magnetometers*, Space Science Reviews **199**, 189 (2016).

[52] R. B. Torbert, C. T. Russell, W. Magnes, R. E. Ergun, P. A. Lindqvist, O. LeContel, H. Vaith, J. Macri, S. Myers, D. Rau, J. Needell, B. King, M. Granoff, M. Chutter, I. Dors, G. Olsson, Y. V. Khotyaintsev, A. Eriksson, C. A. Kletzing, S. Bounds, B. Anderson, W. Baumjohann, M. Steller, K. Bromund, G. Le, R. Nakamura, R. J. Strangeway, H. K. Leinweber, S. Tucker, J. Westfall, D. Fischer, F. Plaschke, J. Porter, and K. Lappalainen, *The FIELDS Instrument Suite on MMS: Scientific Objectives, Measurements, and Data Products*, Space Science Reviews **199**, 105 (2016).

[53] C. Pollock, T. Moore, A. Jacques, J. Burch, U. Gliese, Y. Saito, T. Omoto, L. Avanov, A. Barrie, V. Coffey, J. Dorelli, D. Gershman, B. Giles, T. Rosnack, C. Salo, S. Yokota, M. Adrian, C. Aoustin, C. Auletti, S. Aung, V. Bigio, N. Cao, M. Chandler, D. Chornay, K. Christian, G. Clark, G. Collinson, T. Corris, A. De Los Santos, R. Devlin, T. Diaz, T. Dickerson, C. Dickson, A. Diekmann, F. Diggs, C. Duncan, A. Figueroa-Vinas, C. Firman, M. Freeman, N. Galassi, K. Garcia, G. Goodhart, D. Guererro, J. Hageman, J. Hanley, E. Hemminger, M. Holland, M. Hutchins, T. James, W. Jones, S. Kreisler, J. Kujawski, V. Lavu, J. Lobell, E. LeCompte, A. Lukemire, E. MacDonald, A. Mariano, T. Mukai, K. Narayanan, Q. Nguyan, M. Onizuka, W. Paterson, S. Persyn, B. Piepgrass, F. Cheney, A. Rager, T. Raghuram, A. Ramil, L. Reichenthal, H. Rodriguez, J. Rouzaud, A. Rucker, Y. Saito, M. Samara, J. A. Sauvaud, D. Schuster, M. Shappirio, K. Shelton, D. Sher, D. Smith, K. Smith, S. Smith, D. Steinfeld, R. Szymkiewicz, K. Tanimoto, J. Taylor, C. Tucker, K. Tull, A. Uhl, J. Vloet, P. Walpole, S. Weidner, D. White, G. Winkert, P. S. Yeh, and M. Zeuch, *Fast Plasma Investigation for Magnetospheric Multiscale*, Space Science Reviews **199**, 331 (2016).

[54] R. E. Denton, B. U. Ö. Sonnerup, C. T. Russell, H. Hasegawa, T. D. Phan, R. J. Strangeway, B. L. Giles, R. E. Ergun, P. A. Lindqvist, R. B. Torbert, J. L. Burch, and S. K. Vines, *Determining L-M-N Current Sheet Coordinates at the Magnetopause From Magnetospheric Multiscale Data*, Journal of Geophysical Research: Space Physics **123**, 2274 (2018).

[55] *See Supplemental Material at [URL Will Be Inserted by Publisher] for Detailed Information on the Minimum Variance Analysis (MVA), Electrostatic Fluctuation Spectra, and the Parameters Used in the Equilibrium Model.*

[56] A. C. Fletcher, C. Crabtree, G. Ganguli, D. Malaspina, E. Tejero, and X. Chu, *Kinetic Equilibrium and Stability Analysis of Dipolarization Fronts*, Journal of Geophysical Research: Space Physics **124**, 2010 (2019).

[57] C. Crabtree, G. Ganguli, A. M. DuBois, A. Fletcher, and A. Sen, Kinetic Equilibria of Compressed Current Sheets with Sheared Flows, 2022.

[58] G. Ganguli, Y. C. Lee, and P. J. Palmadesso, *Electron-Ion Hybrid Mode Due to Transverse Velocity Shear*, Physics of Fluids **31**, 2753 (1988).

[59] H. Romero, G. Ganguli, Y. C. Lee, and P. J. Palmadesso, *Electron–Ion Hybrid Instabilities Driven by Velocity Shear in a Magnetized Plasma*, Phys. Fluids B **4**, 1708 (1992).

[60] A. Matsubara and T. Tanikawa, *Anomalous Cross-Field Transport of Electrons Driven by the Electron-Ion Hybrid Instability Due to the Velocity Shear in a Magnetized Filamentary Plasma*, Japanese Journal of Applied Physics **39**, 4920 (2000).

[61] T. A. S. Kumar, S. K. Mattoo, and R. Jha, *Plasma Diffusion across Inhomogeneous Magnetic Fields*, Phys. Plasmas **9**, 2946 (2002).

[62] J. Egedal, A. Le, and W. Daughton, *A Review of Pressure Anisotropy Caused by Electron Trapping in Collisionless Plasma, and Its Implications for Magnetic Reconnection*, Physics of Plasmas **20**, 061201 (2013).

[63] A. Le, J. Egedal, W. Daughton, W. Fox, and N. Katz, *Equations of State for Collisionless Guide-Field Reconnection*, Physical Review Letters **102**, 085001 (2009).

[64] G. Ganguli, C. Crabtree, A. C. Fletcher, E. Tejero, D. Malaspina, and I. Cohen, *Kinetic Equilibrium of Dipolarization Fronts*, Scientific Reports **8**, 17186 (2018).